INSTITUTE OF PHYSICS PUBLISHING PHYSICS IN MEDICINE AND BIOLOGY

Phys. Med. Biol. **49** (2004) 2129–2143 PII: S0031-9155(04)69762-4

On two versions of a 3π algorithm for spiral CT

Alexander Katsevich

Department of Mathematics, University of Central Florida, Orlando, FL 32816-1364, USA

E-mail: akatsevi@pegasus.cc.ucf.edu

Received 1 October 2003
Published 19 May 2004
Online at stacks.iop.org/PMB/49/2129
DOI: 10.1088/0031-9155/49/11/001

Abstract

A 3π algorithm is obtained in which all the derivatives are confined to a detector array. Distance weighting of backprojection coefficients of the algorithm is studied. A numerical experiment indicates that avoiding differentiation along the source trajectory improves spatial resolution. Another numerical experiment shows that the terms depending on the non-standard distance weighting $1/|x - y(s)|$ can no longer be ignored.

1. Introduction

Using redundant data is important in spiral CT. It leads to the reduction of motion and sampling artefacts, efficient use of the applied dose, etc (Bontus *et al* 2001, Köhler *et al* 2002). In Katsevich (2003, 2004) a theoretically exact shift-invariant FBP-type algorithm for spiral CT was proposed that allows one to use redundant data. A closely related quasi-exact algorithm was proposed in Bontus *et al* (2003a, 2003b). The algorithms operate in the 3π mode and require a detector array, which is about three times as large as that required for 1π algorithms (see, e.g., Proksa *et al* (2000), Katsevich (2002)). This aspect of 3π algorithms is very important in medical applications of CT. The reason is that as the number of detector rows and gantry rotation speed continue to increase, 1π algorithms will reach their limitation. Consider a next generation 64 slice scanner, whose gantry makes three revolutions per second. Using table 1 of Noo *et al* (2003) we see that maximum detector utilization with a 1π algorithm is achieved when the table feed equals 6.58 cm per rotation. This translates into the table speed of about 20 cm s^{-1}, which is too high for many patients. 3π algorithms will allow one to slow the table down, but still maintain high detector utilization.

Similarly to the 1π case (see Katsevich 2002), 3π algorithms also admit two versions. Version 1 requires differentiation along the source trajectory. In version 2 all derivatives are confined to the detector array. Since detector sampling is usually much finer than sampling of the source trajectory, it is reasonable to expect that the second version will provide better spatial resolution. The main purpose of this paper is to derive the second version of the 3π algorithm of Katsevich (2004) and to investigate how the resulting backprojection coefficients

depend on distance weighting. We show that similarly to the 1π case two weights are needed to backproject the filtered cone beam projections: $1/|x - y(s)|$ and $1/|x - y(s)|^2$. Here $|x - y(s)|$ denotes the distance from the focal point $y(s)$ to the reconstruction point x. A preliminary numerical experiment presented in the paper indicates that the second version of the 3π algorithm provides better spatial resolution (at least, in the current implementation). Another numerical experiment shows that, as opposed to the 1π case (see Katsevich *et al* 2003), the terms depending on the non-standard distance weighting $1/|x - y(s)|$ can no longer be ignored.

Note that the numerical implementations of the two versions of the 3π algorithm have not been optimized. In particular, all convolutions are performed with respect to the polar angle γ. This is the most obvious approach, but its downside is the need for excessive interpolation, which results in reduced spatial resolution. Recently, F Noo, J Pack and D Heuscher proposed a very efficient and accurate method of implementing version 1 of the 1π algorithm of Katsevich (2002) (see Noo *et al* 2003). One of the features in their approach is that the convolutions are performed with respect to a 'native' coordinate on the detector. This and other improvements resulted in a significant increase in efficiency, spatial resolution and overall image quality. It is quite clear that most of these ideas can be applied to version 1 of the 3π algorithm. The application of the ideas to version 2 of the 3π algorithm is more challenging. Thus, finding optimal implementations of the two versions of the 3π algorithm and a detailed investigation of their numerical performance will be the subject of future research. The purpose of the numerical experiments presented in this paper is only to demonstrate that version 2 of the 3π algorithm works and, given comparable implementations, appears to provide better spatial resolution than version 1.

2. The 3π algorithm

First we introduce the necessary notations. Let

$$C := \{y \in \mathbb{R}^3 : y_1 = R\cos(s),\ y_2 = R\sin(s),\ y_3 = s(h/2\pi),\ s \in \mathbb{R}\} \qquad h > 0 \tag{2.1}$$

be a spiral, and U be an open set strictly inside the spiral:

$$\overline{U} \subset \left\{x \in \mathbb{R}^3 : x_1^2 + x_2^2 < r^2\right\} \qquad 0 < r < R. \tag{2.2}$$

S^2 is the unit sphere in $\mathbb{R}^3$, and

$$D_f(y, \beta) := \int_0^\infty f(y + \beta t)\,\mathrm{d}t \qquad \beta \in S^2 \tag{2.3}$$

$$\beta(s, x) := \frac{x - y(s)}{|x - y(s)|} \qquad x \in U, s \in \mathbb{R} \tag{2.4}$$

that is $D_f(y, \beta)$ is the cone beam transform of f. Also, $\dot{y}(s) := \mathrm{d}y/\mathrm{d}s$. For $\beta \in S^2$, $\beta^\perp$ denotes the great circle $\{\alpha \in S^2 : \alpha \cdot \beta = 0\}$. In what follows it is assumed that $r/R < 0.618$.

Suppose that the x-ray source is fixed at $y(s_0)$ for some $s_0 \in \mathbb{R}$. Since the detector array rotates together with the source, the detector plane depends on s_0 and is denoted by $DP(s_0)$. It is assumed that $DP(s_0)$ is parallel to the axis of the spiral and is tangent to the cylinder $y_1^2 + y_2^2 = R^2$ (cf (2.1)) at the point opposite to the source. Thus, the distance between $y(s_0)$ and the detector plane is $2R$ (see figure 1). Introduce coordinates in the detector plane as follows. Let the d_1-axis be perpendicular to the axis of the spiral, the d_2-axis be parallel to it and the origin coincide with the projection of $y(s_0)$. Project stereographically the upper and

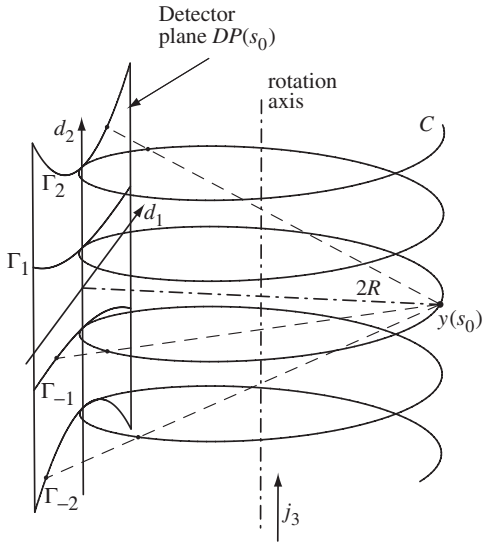

Figure 1. Stereographic projection of the spiral onto the detector plane.

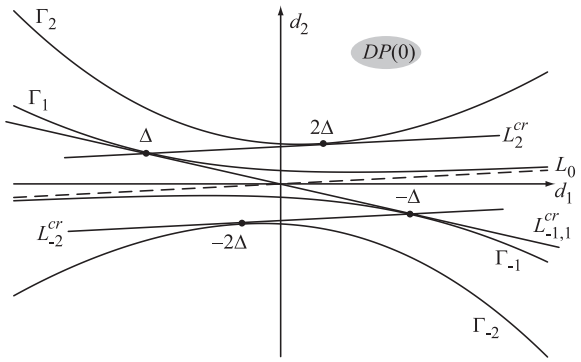

Figure 2. Detector plane with various projections and important lines shown.

lower turns of the spiral onto the detector plane as shown in figure 1. This gives the following parametric curves:

$$\begin{aligned} &d_1(s) = 2R\frac{\sin(s-s_0)}{1-\cos(s-s_0)} && d_2(s) = \frac{h}{\pi}\frac{s-s_0}{1-\cos(s-s_0)} \\ &\rho + 2\pi(j-1) \leqslant s - s_0 \leqslant 2\pi j - \rho && j \geqslant 1 \qquad \text{or} \\ &\rho + 2\pi j \leqslant s - s_0 \leqslant 2\pi(j+1) - \rho && j \leqslant -1 \end{aligned} \tag{2.5}$$

where ρ is determined by radius of support of the object: $\rho = 2\cos^{-1}(r/R)$ (cf (2.2)). These curves are denoted by Γ_j, $j = \pm 1, \pm 2, \ldots$ (see figure 2). L_0 is the projection of the spiral tangent, and $L_{\pm 2}^{\mathrm{cr}}$ are lines parallel to L_0 and tangent to $\Gamma_{\pm 2}$, respectively. $L_{-1,1}^{\mathrm{cr}}$ is the line tangent to both Γ_1 and Γ_{-1}. The quantity Δ is determined as the unique solution of $\tan\Delta = \Delta, \pi < \Delta < 3\pi/2$ (cf Katsevich 2004).

Let $\hat{x}$ denote the projection of x. Sometimes we will write $\hat{x}(s)$ to emphasize that the location of $\hat{x}$ on $DP(s)$ depends on the source position $y(s)$. As is well known, $\hat{x}(s)$ is between

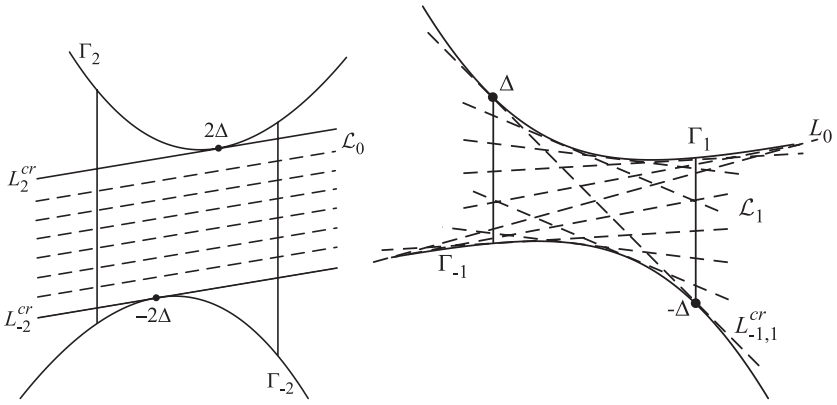

Figure 3. Family $\mathcal{L}_0$ of filtering lines parallel to the spiral tangent (left-hand panel) and family $\mathcal{L}_1$ of filtering lines tangent to $\Gamma_{\pm 1}$ (right-hand panel).

Γ_{-1} and Γ_1 if and only if $s \in I^{1\pi}(x)$. Here $I^{1\pi}(x) := [b^{1\pi}(x), t^{1\pi}(x)]$ is the 1π parametric interval of x. The region on the detector bounded by Γ_{-1} and Γ_1 is known in the literature as 1π or Tam–Danielsson window (Tam 1995, Tam *et al* 1998, Danielsson *et al* 1997). In a similar fashion, the region between Γ_{-2} and Γ_2 is called the 3π window (Katsevich 2004). Let $I^{3\pi}(x)$ be the parametric interval such that $\hat{x}(s)$ is inside the 3π window if and only if $s \in I^{3\pi}(x)$. The corresponding section of the spiral is denoted by $C^{3\pi}(x)$. It is shown in Proksa *et al* (2000) and Katsevich (2004) that $I^{3\pi}(x)$ is either a single interval $I^{3\pi}(x) = \left[b_1^{3\pi}, t_1^{3\pi}\right]$ or consists of three subintervals $I^{3\pi}(x) = \cup_{i=1}^{3}\left[b_i^{3\pi}, t_i^{3\pi}\right]$ (here we use the notation slightly different from that of Katsevich (2004).

Now define three families of filtering lines. The first family, which consists of lines parallel to L_0, is denoted by $\mathcal{L}_0$ (see figure 3, left-hand panel). The second family, which consists of lines tangent to $\Gamma_{\pm 1}$, is denoted by $\mathcal{L}_1$ (see figure 3, right-hand panel).

Let $\psi(t)$ be any smooth function with the properties $\psi(0) = 0$, $\psi'(t) > 0, t \in \mathbb{R}$. Define the family of lines $\mathcal{L}_2$ by requesting that any given $L \in \mathcal{L}_2$ has three points of intersection with $\Gamma_{\pm 1} \cup \Gamma_{\pm 2}$: s_1, s_2, s_3, and these points satisfy

$$\begin{cases} s_1 - s = \psi(s_3 - s_2) & s + 2\pi < s_3 < s + 4\pi \\ s_2 - s_3 = \psi(s - s_1) & s - 4\pi < s_3 < s - 2\pi. \end{cases} \tag{2.6}$$

The requirement that s_1, s_2, s_3 belong to a line reduces the number of degrees of freedom from three to two. Equation (2.6) further reduces this number to one. Consequently, the lines $L \in \mathcal{L}_2$ can be parametrized by only one parameter. One can use, for example, s_3, $2\pi < |s_3| < 4\pi$. The location of the intersection points depends on where s_3 is and is illustrated in figure 4. Top half of the family $\mathcal{L}_2$ that is obtained by choosing $\psi(t) = t$ in (2.6) is shown in figure 5. One has that $\hat{x} \to L_2^{\mathrm{cr}}$ implies $L \to L_2^{\mathrm{cr}}$. Similarly, $\hat{x} \to L_{-2}^{\mathrm{cr}}$ implies $L \to L_{-2}^{\mathrm{cr}}$.

Figure 6 summarizes which filtering lines are used depending on where $\hat{x}$ is inside the 3π window, provided that $\hat{x}$ is above L_0. If $\hat{x}$ is below L_0, then the filtering lines are obtained from figure 6 using symmetry about the origin.

Given x and a source position $y(s)$, $s \in I^{3\pi}(x)$, find a filtering line $L \in \mathcal{L}_k, k = 0, 1, 2$, containing $\hat{x}$. The point and line determine the plane $\Pi(s, x)$. Let $u_k(s, x)$ be the unit vector perpendicular to $\Pi(s, x)$ and pointing up (i.e. in the direction of the spiral motion). Denote

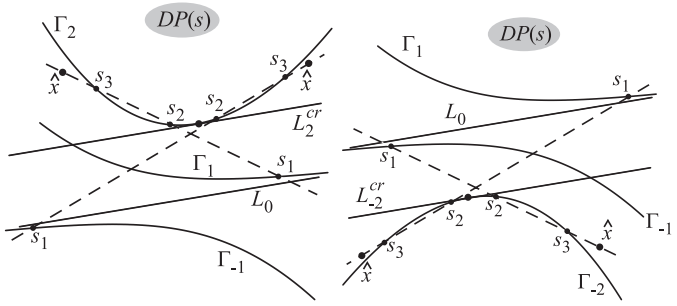

Figure 4. Four possible locations of a line $L_2 \in \mathcal{L}_2$ used in the algorithm. Left-hand panel illustrates the cases $2\pi < s_3 - s < 2\Delta$ and $2\Delta < s_3 - s < 4\pi$. Right-hand panel illustrates the cases $-4\pi < s_3 - s < -2\Delta$ and $-2\Delta < s_3 - s < -2\pi$.

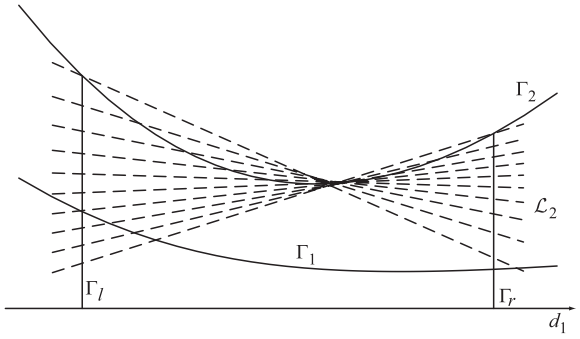

Figure 5. Top half of the family $\mathcal{L}_2$ that is obtained by choosing $\psi(t) = t$ in (2.6).

$e_k(s, x) = \beta(s, x) \times u_k(s, x)$. As follows from the construction (see figure 6), vectors $e_k(s, x)$ and $u_k(s, x)$ depend only on s and $\beta(s, x)$. The 3π algorithm is given by the formula

$$\begin{aligned} f(x) &= -\frac{1}{4\pi^2} \int_{I^{3\pi}(x)} \frac{1}{|x - y(s)|} \sum_{m=1}^{M(s,\beta(s,x))} F_m(s, \beta(s, x))\, \mathrm{d}s \\ F_m(s, \beta) &:= c_m(s, \beta) \int_0^{2\pi} \frac{\partial}{\partial q} D_f(y(q), \Theta_{k_m}(s, \beta, \gamma))|_{q=s} \frac{\mathrm{d}\gamma}{\sin\gamma} \\ \Theta_k(s, \beta, \gamma) &:= \cos\gamma\beta + \sin\gamma e_k(s, \beta). \end{aligned} \tag{2.7}$$

If $\hat{x}$ is between Γ_1 and Γ_{-1}, then $M(s, \beta(s, x)) = 3$ (see figure 6, two bottom panels). In this case $k_1 = 0$ (i.e. a line from $\mathcal{L}_0$ is used) and $k_2 = k_3 = 1$ (i.e. two lines from $\mathcal{L}_1$ are used). If $\hat{x}$ is between Γ_1 and Γ_2 or between Γ_{-1} and Γ_{-2}, then $M(s, \beta(s, x)) = 1$ (see figure 6, three top panels). In this case $k_1 = 0$ when $\hat{x}$ is between L_2^{cr} and L_{-2}^{cr} (a line from $\mathcal{L}_0$ is used), and $k_1 = 2$ when $\hat{x}$ is outside the two lines (a line from $\mathcal{L}_2$ is used). The corresponding backprojection coefficients c_m are also given in the figure. As is easily seen, (2.7) defines a convolution-based filtered backprojection algorithm.

3. The second version of the 3π algorithm

In this section, we will continue the convention that subscript $k = 0, 1, 2$ indicates the family of filtering lines using which the corresponding quantity is computed. Denote

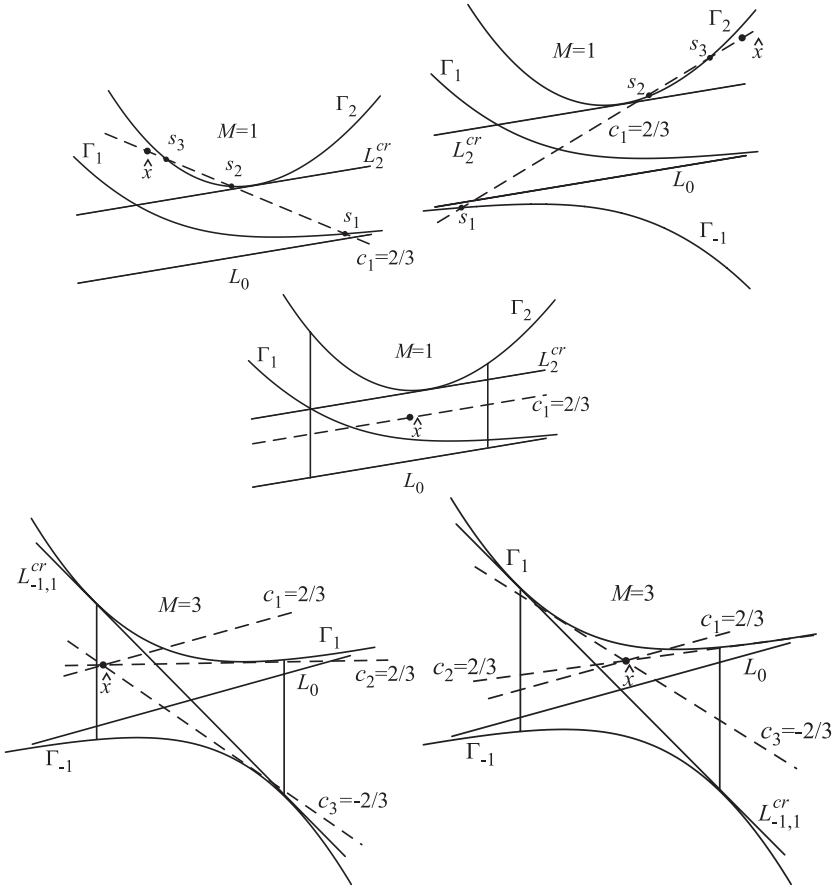

Figure 6. An illustration of how to choose filtering lines (shown as dashed lines) and the corresponding backprojection coefficients c_m in various cases when x is projected above L_0.

$$\begin{aligned}
\Psi_{1k}(s,\beta) &= \int_0^{2\pi} D_f(y(s),\Theta_k(s,\beta,\gamma))\frac{\mathrm{d}\gamma}{\sin\gamma}\\
\Psi_{2k}(s,\beta) &= \int_0^{2\pi} \left(\nabla_{u_k(s,\beta)}D_f\right)(y(s),\Theta_k(s,\beta,\gamma))\cot(\gamma)\,\mathrm{d}\gamma\\
\Psi_{3k}(s,\beta) &= \int_0^{2\pi} \left(\nabla_{u_k(s,\beta)}D_f\right)(y(s),\Theta_k(s,\beta,\gamma))\,\mathrm{d}\gamma\\
\Psi_{4k}(s,\beta) &= \int_0^{2\pi} \left(\frac{\partial}{\partial\gamma}D_f(y(s),\Theta_k(s,\beta,\gamma))\right)\frac{\mathrm{d}\gamma}{\sin\gamma} \qquad k=0,1,2.
\end{aligned} \tag{3.1}$$

Here $\nabla_u D_f$ denotes the derivative of D_f with respect to the angular variables along the direction u:

$$(\nabla_u D_f)(y(s),\Theta) = \frac{\partial}{\partial t}D_f\left(y(s),\sqrt{1-t^2}\Theta+tu\right)\Big|_{t=0} \qquad \Theta\in u^{\perp}. \tag{3.2}$$

Denote also

$$\begin{aligned}
\mu_{1k}(s,x) &= \frac{\partial}{\partial s}\frac{1}{|x-y(s)|} & \mu_{2k}(s,x) &= \frac{\beta_s'(s,x)\cdot u_k(s,x)}{|x-y(s)|}\\
\mu_{3k}(s,x) &= \frac{(e_k)_s'(s,x)\cdot u_k(s,x)}{|x-y(s)|} & \mu_{4k}(s,x) &= \frac{\beta_s'(s,x)\cdot e_k(s,x)}{|x-y(s)|}.
\end{aligned} \tag{3.3}$$

Here $\beta_s' = \partial\beta/\partial s$ and $e_s' = \partial e/\partial s$.

Integrating by parts with respect to s in (2.7) similarly to Katsevich (2002), we obtain an inversion formula in which all the derivatives are performed with respect to the angular variables.

$$\begin{aligned}
f(x) = -\frac{1}{4\pi^2}\Bigg\{ &\sum_{i=1}^{N^{3\pi}(x)} \frac{c_2(s,\beta)\Psi_{12}(s,\beta)}{|x-y(s)|}\Bigg|_{s=b_i^{3\pi}(x)}^{s=t_i^{3\pi}(x)}\\
&- \int_{I^{3\pi}(x)} \sum_{m=1}^{M(s,\beta)} c_m(s,\beta)\sum_{j=1}^{4}\mu_{jk_m}(s,x)\Psi_{jk_m}(s,\beta)\,\mathrm{d}s\Bigg\} \qquad \beta=\beta(s,x)
\end{aligned} \tag{3.4}$$

where $N^{3\pi}(x)$ equals either 1 or 3, depending on how many subintervals $I^{3\pi}(x)$ consists of.

Let us recall that (3.4) is obtained by substituting the identity

$$\frac{\partial}{\partial q}D_f(y(q),\Theta(s,x,\gamma))|_{q=s} = \frac{\partial}{\partial s}D_f(y(s),\Theta(s,x,\gamma)) - \frac{\partial}{\partial q}D_f(y(s),\Theta(q,x,\gamma))|_{q=s} \tag{3.5}$$

into (2.7) and integrating the first term by parts with respect to s. To avoid differentiating a discontinuous function, we represent the integral over $I^{3\pi}(x)$ as a sum of integrals over smaller subsets of $I^{3\pi}(x)$ such that all functions in (2.7) are continuous inside these subsets. By construction, a discontinuity may occur when one of the following happens: $\hat{x}(s)$, $s\in I^{3\pi}(x)$, intersects $\Gamma_{\pm1}$, $L^{\mathrm{cr}}_{\pm2}$, $L^{\mathrm{cr}}_{-1,1}$ or $\Gamma_{\pm2}$.

Consider now each of these cases. When $\hat{x}(s)\to\Gamma_{\pm1}$ from inside of the 1π window, the two filtering lines $L\in\mathcal{L}_1$ through $\hat{x}(s)$ approach each other. Since the corresponding backprojection coefficients are $c_2 = 2/3$ and $c_3 = -2/3$, the contributions of these filtering lines cancel each other when $\hat{x}(s)\in\Gamma_{\pm1}$. Consequently, the corresponding boundary term that arises after integration by parts equals zero.

When $\hat{x}(s)$ intersects L^{cr}_2, we have to switch from one family of filtering lines to another (say, from $\mathcal{L}_0$ to $\mathcal{L}_2$). However, both the limiting filtering lines and the corresponding backprojection coefficients are the same regardless of the direction from which $\hat{x}(s)$ approaches L^{cr}_2. Let s_0 be such that $\hat{x}(s_0)\in L^{\mathrm{cr}}_2$. Our argument implies that the boundary terms which arise after integration by parts on each side of s_0 cancel each other. The same cancellation occurs when $\hat{x}(s)$ intersects L^{cr}_{-2}.

When $\hat{x}(s)$ intersects $L^{\mathrm{cr}}_{-1,1}$, the tangency point of one of the two filtering lines $L\in\mathcal{L}_1$ experiences a jump. As before, the limiting filtering lines and the backprojection coefficients c_3 (see two bottom panels of figure 6) are the same regardless of the direction from which $\hat{x}(s)$ approaches $L^{\mathrm{cr}}_{-1,1}$. Consequently, no boundary terms arise from this discontinuity as well.

Thus, boundary terms arise only when $\hat{x}(s)$ intersects $\Gamma_{\pm2}$, i.e. when s coincides with the boundary of $I^{3\pi}(x)$. Because of this analysis, we can assume in what follows that all quantities are locally continuous.

Denote for convenience $L := |x - y(s)|$. For future references we state here the following useful formulae:

$$\mu_{1k} = \frac{\partial}{\partial s}\frac{1}{|x - y(s)|} = \frac{\beta \cdot \dot{y}(s)}{L^2} \tag{3.6}$$

and

$$\beta_s'(s, x) = \frac{\partial}{\partial s}\frac{x - y(s)}{|x - y(s)|} = \frac{-\dot{y}(s) + \beta(\beta \cdot \dot{y}(s))}{L}. \tag{3.7}$$

Here and in what follows $\beta = \beta(s, x)$. In this section we omit the subscript of e_k and u_k, because it will be clear from the context which family of filtering lines is discussed. From (3.3), μ_{1k} is independent of k and is determined using (3.6).

The remaining backprojection coefficients for lines $L \in \mathcal{L}_0$ are easy to find. Since the filtering direction is parallel to the spiral tangent, we get

$$u(s, x) = \frac{\dot{y}(s) \times \beta}{|\dot{y}(s) \times \beta|} \qquad e = \beta \times u = \frac{\dot{y}(s) - \beta(\beta \cdot \dot{y}(s))}{|\dot{y}(s) \times \beta|}. \tag{3.8}$$

Using (3.7) and (3.8) we compute

$$\beta_s' \cdot u = 0 \qquad \beta_s' \cdot e = \frac{-|\dot{y}(s)|^2 + (\beta \cdot \dot{y}(s))^2}{L|\dot{y}(s) \times \beta|} = -\frac{|\dot{y}(s) \times \beta|}{L}. \tag{3.9}$$

By construction, $e \perp u$, $\beta \perp u$ and $\beta' \cdot u = 0$ (see (3.7) and (3.8)). Therefore

$$e_s' \cdot u = \frac{\ddot{y}(s) \cdot u}{|\dot{y}(s) \times \beta|}. \tag{3.10}$$

Next, pick a line $L \in \mathcal{L}_1$. Let $s_t := s_t(s, x)$ be the point where the plane containing x, $y(s)$, and L is tangent to $C^{3\pi}(x)$. Denote

$$v(s, x) := (y(s) - x) \times (y(s_t) - x)\delta. \tag{3.11}$$

Here $\delta = +1$ or $\delta = -1$ to guarantee that $v(s, x)$ always points along the spiral motion. Clearly, $u(s, x) = v(s, x)/|v(s, x)|$ and, using (3.7),

$$\beta_s' \cdot u = -\frac{\dot{y}(s) \cdot u}{L} \qquad \beta_s' \cdot e = -\frac{\dot{y}(s) \cdot e}{L}. \tag{3.12}$$

Differentiation of (3.11) with respect to s gives

$$\begin{aligned} v_s'(s, x) &= \left[\dot{y}(s) \times (y(s_t) - x) + (y(s) - x) \times \dot{y}(s_t)\frac{\partial s_t}{\partial s}\right]\delta \\ &= [\dot{y}(s) \times (y(s_t) - x)]\delta + \text{const}\, v. \end{aligned} \tag{3.13}$$

Here we have assumed that δ is locally a constant (cf the remark preceding (3.6)). Therefore,

$$\begin{aligned} e \cdot u_s' &= \frac{\{\beta \times [-\beta L \times (y(s_t) - x)]\} \cdot \{\dot{y}(s) \times (y(s_t) - x)\}}{|v|^2} \\ &= \frac{L}{|v|^2}\{(y(s_t) - x) - \beta[\beta \cdot (y(s_t) - x)]\} \cdot \{\dot{y}(s) \times (y(s_t) - x)\} \\ &= -\frac{L}{|v|^2}[\beta \cdot (y(s_t) - x)]\beta \cdot \{\dot{y}(s) \times (y(s_t) - x)\} \\ &= \frac{\beta \cdot (y(s_t) - x)}{|v|^2}\dot{y}(s) \cdot \{L\beta \times (y(s_t) - x)\} \\ &= [\beta \cdot (x - y(s_t))]\frac{(v \cdot \dot{y}(s))\delta}{|v|^2} = [\beta \cdot (x - y(s_t))]\frac{u \cdot \dot{y}(s)}{|v|}\delta. \end{aligned} \tag{3.14}$$

To find the dependence of this coefficient on L, we transform it further

$$e \cdot u'_s = [\beta \cdot (L\beta + (y(s) - y(s_t)))] \frac{u \cdot \dot{y}(s)}{|L\beta \times (y(s) - y(s_t))|}\delta$$
$$= \left[1 + \frac{\beta \cdot (y(s) - y(s_t))}{L}\right] \frac{u \cdot \dot{y}(s)}{|\beta \times (y(s) - y(s_t))|}\delta. \tag{3.15}$$

Consider now lines $L \in \mathcal{L}_2$. Let s_1, s_2 and s_3 be the points found according to (2.6). Denote similarly to (3.11):

$$v(s, x) := (y(s) - x) \times (y(s_1) - x)\delta. \tag{3.16}$$

Clearly, $u(s, x) = v(s, x)/|v(s, x)|$ and, using (3.7),

$$\beta'_s \cdot u = -\frac{\dot{y}(s) \cdot u}{L} \qquad \beta'_s \cdot e = -\frac{\dot{y}(s) \cdot e}{L}. \tag{3.17}$$

Denote also $V := y(s) - x$, $V_1 := y(s_1) - x$. Thus, assuming as before that δ is constant,

$$v'_s(s, x) = \left[(\dot{y}(s) \times V_1) + (V \times \dot{y}(s_1))\frac{\partial s_1}{\partial s}\right]\delta. \tag{3.18}$$

Starting with the definition of e, we get

$$e \cdot u'_s = \frac{(\beta \times v) \cdot v'_s}{|v|^2} = -\frac{[V \times (V \times V_1)] \cdot \left[(\dot{y}(s) \times V_1) + (V \times \dot{y}(s_1))\frac{\partial s_1}{\partial s}\right]}{|V| \cdot |v|^2}$$
$$= \frac{[|V|^2 V_1 - (V \cdot V_1)V] \cdot \left[(\dot{y}(s) \times V_1) + (V \times \dot{y}(s_1))\frac{\partial s_1}{\partial s}\right]}{|V| \cdot |v|^2}$$
$$= \frac{|V|^2 V_1 \cdot (V \times \dot{y}(s_1))\frac{\partial s_1}{\partial s} - (V \cdot V_1)V \cdot [\dot{y}(s) \times V_1]}{|V| \cdot |v|^2}$$
$$= -\frac{|V|^2 \dot{y}(s_1) \cdot (V \times V_1)\frac{\partial s_1}{\partial s} - (V \cdot V_1)\dot{y}(s) \cdot [V \times V_1]}{|V| \cdot |v|^2}$$
$$= -\frac{\left[|V|^2 \frac{\partial s_1}{\partial s}\dot{y}(s_1) - (V \cdot V_1)\dot{y}(s)\right] \cdot v}{|V| \cdot |v|^2}\delta. \tag{3.19}$$

Recall that $|V| = L$. To find the dependence of this coefficient on L, we transform it further

$$e \cdot u'_s = -\frac{\left[L^2 \frac{\partial s_1}{\partial s}\dot{y}(s_1) + (L\beta \cdot (y(s_1) - y(s) - L\beta))\dot{y}(s)\right] \cdot u}{L \cdot |L\beta \times (y(s_1) - y(s) - L\beta)|}\delta$$
$$= -\frac{\left[\frac{\partial s_1}{\partial s}\dot{y}(s_1) + [(\beta \cdot (y(s_1) - y(s))/L - 1]\dot{y}(s)\right] \cdot u}{|\beta \times (y(s_1) - y(s))|}\delta$$
$$= -\left\{\frac{\left(\frac{\partial s_1}{\partial s}\dot{y}(s_1) - \dot{y}(s)\right) \cdot u}{|\beta \times (y(s_1) - y(s))|} + \frac{1}{L}\frac{(\beta \cdot (y(s_1) - y(s))(\dot{y}(s) \cdot u)}{|\beta \times (y(s_1) - y(s))|}\right\}\delta. \tag{3.20}$$

The final step is to study how $\partial s_1/\partial s$ depends on L. This will be done analogously to Katsevich (2002). For convenience, introduce the quantities $\Delta_i := s_i - s$, $s = 1, 2, 3$. By construction, we can regard Δ_3 as a function of Δ_1, and $\Delta_1 = \Delta_1(s)$ (for the latter we assume x is fixed). Since L contains $\hat{x}(s)$, we have (cf (27) in Katsevich (2002))

$$\frac{\hat{x}_2(s) - d_2(\Delta_3)}{\hat{x}_1(s) - d_1(\Delta_3)} = \frac{\hat{x}_2(s) - d_2(\Delta_1)}{\hat{x}_1(s) - d_1(\Delta_1)} =: m. \tag{3.21}$$

Here $(\hat{x}_1(s), \hat{x}_2(s))$ are the coordinates of the projection of x onto $DP(s)$, and $(d_1(\Delta), d_2(\Delta))$ are the parametric equations of $\Gamma_{\pm 1}, \Gamma_{\pm 2}$. Restricting $|\Delta|$ to $(0, 2\pi)$ and $(2\pi, 4\pi)$ gives $\Gamma_{\pm 1}$

and $\Gamma_{\pm 2}$, respectively. Differentiation of (3.21) with respect to s yields

$$\frac{(\hat{x}_2'(s) - d_2'(\Delta_3)\Delta_3'\Delta_1')(\hat{x}_1(s) - d_1(\Delta_3)) - (\hat{x}_2(s) - d_2(\Delta_3))(\hat{x}_1'(s) - d_1'(\Delta_3)\Delta_3'\Delta_1')}{(\hat{x}_1(s) - d_1(\Delta_3))^2}$$
$$= \frac{(\hat{x}_2'(s) - d_2'(\Delta_1)\Delta_1')(\hat{x}_1(s) - d_1(\Delta_1)) - (\hat{x}_2(s) - d_2(\Delta_1))(\hat{x}_1'(s) - d_1'(\Delta_1)\Delta_1')}{(\hat{x}_1(s) - d_1(\Delta_1))^2} \tag{3.22}$$

where $\Delta_3' = \mathrm{d}\Delta_3(\Delta_1)/\mathrm{d}\Delta_1$ and $\Delta_1' = \mathrm{d}\Delta_1(s)/\mathrm{d}s$. Simplification of (3.22) gives

$$\frac{1}{\hat{x}_1(s) - d_1(\Delta_3)}((\hat{x}_2'(s) - d_2'(\Delta_3)\Delta_3'\Delta_1') - m(\hat{x}_1'(s) - d_1'(\Delta_3)\Delta_3'\Delta_1'))$$
$$= \frac{1}{\hat{x}_1(s) - d_1(\Delta_1)}((\hat{x}_2'(s) - d_2'(\Delta_1)\Delta_1') - m(\hat{x}_1'(s) - d_1'(\Delta_1)\Delta_1')). \tag{3.23}$$

Solving for Δ_1' we get

$$\Delta_1' = \frac{(\hat{x}_2'(s) - m\hat{x}_1'(s))(1-a)}{\Delta_3'(d_2'(\Delta_3) - md_1'(\Delta_3)) - a(d_2'(\Delta_1) - md_1'(\Delta_1))} \tag{3.24}$$

where

$$a := \frac{\hat{x}_1(s) - d_1(\Delta_3)}{\hat{x}_1(s) - d_1(\Delta_1)}. \tag{3.25}$$

As follows from figure 4 and (2.6), Δ_3 is an increasing function of Δ_1. Assuming the contrary, we get from figure 4 that $s_3 - s_2$ gets smaller when $s_1 - s$ is increased, which contradicts the assumption $\psi' > 0$. Hence $\Delta_3' > 0$. Using figure 4 again it is now easy to see that the denominator in (3.24) is not zero when $\hat{x}$ is between L_2^{cr} and Γ_2 or between L_{-2}^{cr} and Γ_{-2}.

As follows from Katsevich (2002), $\hat{x}_{1,2}'(s) = A_{1,2}(\beta) + B_{1,2}(\beta)/L$. Clearly, all other quantities in (3.24) do not depend on L. Since $\partial s_1/\partial s = 1 + \Delta_1'(s)$, combining (3.24) with (3.20) proves that

$$e \cdot u_s' = A + \frac{B}{L} \tag{3.26}$$

for some A and B that do not depend on L.

Let us now summarize the obtained results. We have

$$\begin{array}{lll} \mu_{20} = 0 & \mu_{30} = \dfrac{\ddot{y}(s)\cdot u_0}{|\dot{y}(s)\times\beta|}\dfrac{1}{L} & \mu_{40} = -\dfrac{|\dot{y}(s)\times\beta|}{L^2} \\ \mu_{2k} = -\dfrac{\dot{y}(s)\cdot u_k}{L^2} & \mu_{3k} = \dfrac{A_k}{L} + \dfrac{B_k}{L^2} & \mu_{4k} = -\dfrac{\dot{y}(s)\cdot e_k}{L^2} \quad k = 1, 2. \end{array} \tag{3.27}$$

Here A_k and B_k are some quantities that depend only on s and $\beta(s, x)$. Combining (3.4) with (3.27) we see that most of the terms are backprojected using the factor L^{-2}. However, the boundary term and the terms containing Ψ_{3k} are backprojected using both L^{-1} and L^{-2}.

Comparing (2.7) with (3.1) and (3.4) we see that version 2 requires only about two times more filtering than version 1. First, $\mu_{20} = 0$. Second, calculation of Ψ_{3k} involves simple integration, which is an $O(N)$ operation. In contrast, computation of a convolution using FFT requires $O(N \log_2 N)$ operations. With $N \gtrsim 1024$, the computational expense of integration is much smaller compared with that of convolution. Similarly, Ψ_{1k} can be computed from Ψ_{4k} using integration. From (3.27), version 2 requires two backprojections. However, most of the computational expense (e.g., projecting x onto the detector, computing the distance $|x - y(s)|$ etc) is shared by the two backprojections. Finally, version 2 requires calculation of the boundary terms. For a given x, these terms are computed only when the current source position is close to the boundary of $I^{3\pi}(x)$. Hence, the associated computational expense is not significant. This argument allows us to estimate that version 2 should not be more than two times slower than version 1.

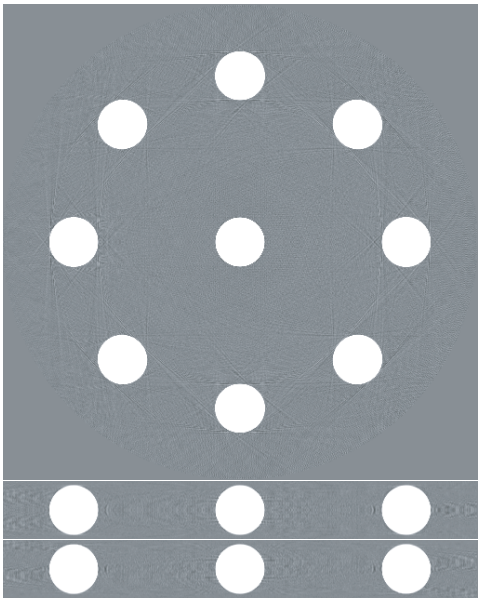

Figure 7. Reconstruction of the nine-ball phantom using version 1 of the 3π algorithm. Grey level window—$[-0.5, 0.5]$.

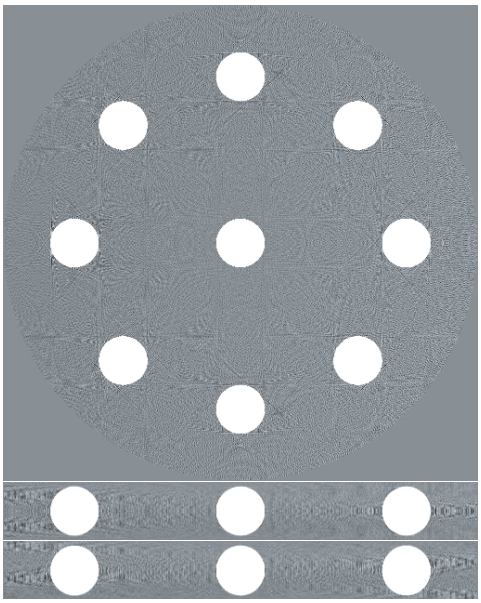

Figure 8. Reconstruction of the nine-ball phantom using version 2 of the 3π algorithm. Grey level window—$[-0.5, 0.5]$.

4. Numerical experiments

Version 1 of the algorithm is based on equation (2.7). Let $D_f(s, d_1, d_2)$ denote the cone beam data on the flat detector array, and $\Theta(s, d_1, d_2)$ be the unit vector pointing from the source at

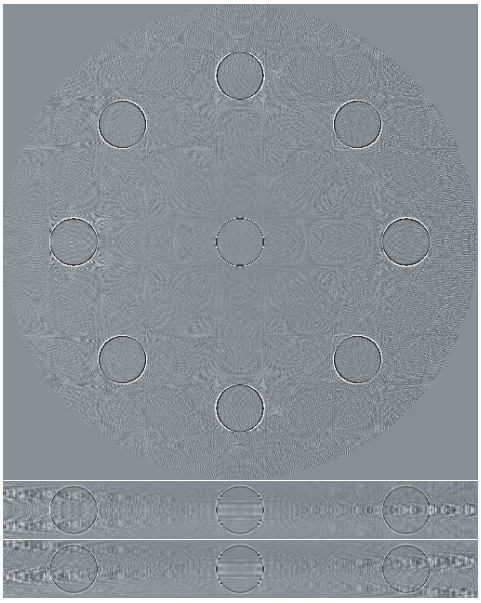

Figure 9. The difference between the results in figures 7 and 8. Grey level window—[−0.5, 0.5].

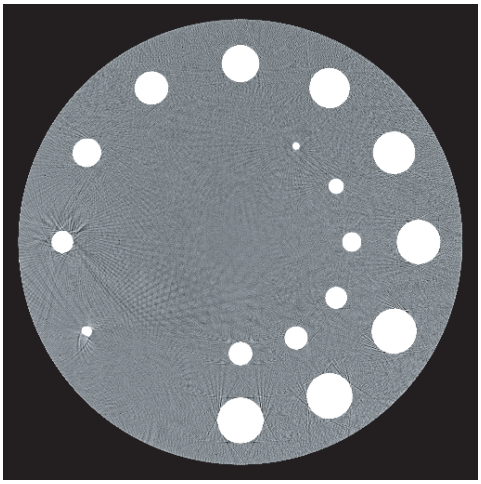

Figure 10. Complete reconstruction of the clock phantom. Grey level window—[0.95, 1.05].

$y(s)$ towards the point on the detector with coordinates (d_1, d_2). Then one has (see (86) in Noo *et al* (2003)):

$$\frac{\partial}{\partial q} D_f(y(q), \Theta(s, d_1, d_2))\bigg|_{q=s} = \frac{\partial D_f(s, d_1, d_2)}{\partial s} + \frac{d_1^2 + (2R)^2}{2R} \frac{\partial D_f(s, d_1, d_2)}{\partial d_1} + \frac{d_1 d_2}{2R} \frac{\partial D_f(s, d_1, d_2)}{\partial d_2}. \tag{4.1}$$

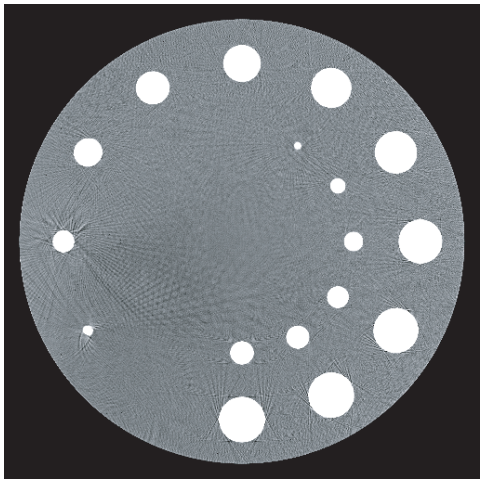

Figure 11. Reconstruction of the clock phantom without Ψ_{3k} terms. Grey level window—[0.95, 1.05].

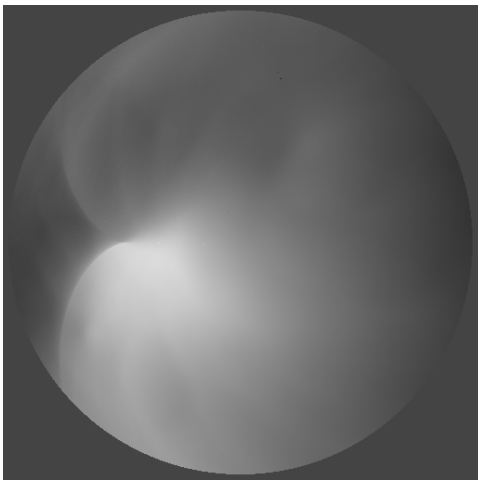

Figure 12. The combined image of Ψ_{3k} terms. Grey level window—[−0.004, 0.011].

Here we have used that the source–detector distance is $2R$. The actual derivative $\partial/\partial q$ was computed in the code using a finite-difference approximation of (4.1) (see (87) in Noo *et al* (2003)). Version 2 of the algorithm is based on equation (3.4).

To compare the two versions of the 3π algorithm we performed an experiment with a nine ball phantom. Each ball has density 1 and radius 20 mm. The centres of the balls are 140 mm away from the isocentre. Additional simulation parameters are presented in table 1. Reconstruction results are shown in figure 7 (version 1) and figure 8 (version 2). The difference between the results (version 1 minus version 2) is shown in figure 9. The grey level window is $[-0.5, 0.5]$ in all the figures. In each figure top panel shows xy cross-section, middle panel–xz cross-section and the bottom panel–yz cross-section. As one can easily see from the results, integration by parts results in increased noise and spatial resolution.

Table 1. Simulation parameters in the nine ball experiment.

R (radius of the spiral)	600 mm
h (pitch of the spiral)	66 mm
Detector pixel size in each direction (as projected to isocentre)	0.575×0.5 mm^2
Number of detector rows	256
Number of detectors per row	750
Number of source positions per rotation	900

Table 2. Simulation parameters in the clock phantom experiment.

R (radius of the spiral)	570 mm
h (pitch of the spiral)	46 mm
Detector pixel size in each direction (as projected to isocentre)	0.75 mm
Number of detector rows	128
Number of detectors per row	745
Number of source positions per rotation	1160

To investigate if the terms containing Ψ_{3k} can be omitted from the reconstruction we performed an experiment with the clock phantom. The phantom is a superposition of a cylinder with radius 240 mm and two sets of balls. The first set consists of 12 balls with radius 24 mm, that are placed on a spiral with radius 192 mm and pitch 28.8 mm. The second set consists of 12 balls with radius 12 mm, that are placed on a spiral in the opposite direction with radius 120 mm and pitch 28.8 mm. The cylinder has density 1, and the balls have density 2. Additional simulation parameters are presented in table 2. Complete reconstruction is shown in figure 10. Reconstruction without the Ψ_{3k} terms is shown in figure 11. One can see some low frequency darkening artefact in the area between the isocentre and the ball in the 8 o'clock position. The combined image of all Ψ_{3k} terms is shown in figure 12. Pixel values of that image are within the range $[-0.003, 0.01]$. The results demonstrate that the Ψ_{3k} terms cannot be ignored, as opposed to the 1π case (Katsevich *et al* 2003).

Acknowledgments

This research was supported in part by NSF grant DMS-0104033, Toshiba Medical Systems Corporation, Japan and Bio-Imaging Research, Inc., Illinois, USA.

References

Bontus C, Köhler Th and Proksa R 2003a Exact and quasi exact CT reconstruction algorithms. Extensions of the Katsevich method *Proc. 7th Int. Conf. on Fully 3D Reconstruction in Radiology and Nuclear Medicine (Saint-Malo, 29 June–4 July 2003)* ed Y Bizais

Bontus C, Köhler Th and Proksa R 2003b A quasiexact reconstruction algorithm for helical CT using a 3-PI acquisition *Med. Phys.* **30** 2493–502

Bontus C, Proksa R, Timmer J, Köhler Th and Grass M 2001 Movement artifacts in helical CT cone-beam reconstruction *Proc. Int. Meeting on Fully Three-Dimensional Image Reconstruction in Radiology and Nuclear Medicine (Pacific Grove, CA, 30 Oct.–2 Nov. 2001)* ed R Huesman pp 199–202

Danielsson P E *et al* 1997 Towards exact reconstruction for helical cone-beam scanning of long objects. A new detector arrangement and a new completeness condition *Proc. 1997 Meeting on Fully 3D Image Reconstruction in Radiology and Nuclear Medicine (Pittsburgh)* ed D W Townsend and P E Kinahan pp 141–4

Katsevich A 2002 Analysis of an exact inversion algorithm for spiral cone-beam CT *Phys. Med. Biol.* **47** 2583–98

Katsevich A 2003 A generalized inversion formula for cone beam CT *Proc. 7th Int. Conf. on Fully 3D Reconstruction in Radiology and Nuclear Medicine (Saint-Malo 29 June–4 July 2003)* ed Y Bizais

Katsevich A 2004 3π algorithm for spiral CT (submitted)

Katsevich A, Lauritsch G, Bruder H, Flohr T and Stierstorfer K 2003 Evaluation and empirical analysis of an exact FBP algorithm for spiral cone-beam CT *Proc. SPIE 2003 Medical Imaging Conference* ed M Sonka and J M Fitzpatrick *Proc. SPIE* **5032** 663–74

Köhler Th, Proksa R, Bontus C, Grass M and Timmer J 2002 Artifact analysis of approximate cone-beam CT algorithms *Med. Phys.* **29** 51–64

Noo F, Pack J and Heuscher D 2003 Exact helical reconstruction using native cone-beam geometries *Phys. Med. Biol.* **48** 3787–818

Proksa R, Köhler Th, Grass M and Timmer J 2000 The *n*-PI method for helical conebeam CT *IEEE Trans. Med. Imaging* **19** 848–63

Tam K C 1995 Three-dimensional computerized tomography scanning method and system for imaging large objects with smaller area detectors *US Patent* 5,390,112

Tam K C, Samarasekera S and Sauer F 1998 Exact cone beam CT with a spiral scan *Phys. Med. Biol.* **43** 1015–24